Supporting Information

Fluorinated Pseudo-halide Anion Enables >19% Efficiency and Durable Perovskite Quantum Dot Solar Cells

*Chenyu Zhao, Du Li, Xuliang Zhang, Hehe Huang, Claudio Cazorla, Xinyu Zhao, Huifeng Li, Yuhao Chen, Wei Zhu, Tom Wu, Jianyu Yuan**

C. Zhao, D. Li, X. Zhang, H. Huang, X. Zhao, H. Li, Y. Chen, W. Zhu, Prof. J. Yuan
State Key Laboratory of Bioinspired Interfacial Materials Science, Institute of Functional Nano & Soft Materials (FUNSOM), Soochow University, 199 Ren-Ai Road, Suzhou Industrial Park, Suzhou, Jiangsu 215123, China.
E-mail: jyyuan@suda.edu.cn

Prof. C. Cazorla
Department de Física, Universitat Politècnica de Catalunya, 08034 Barcelona, Spain.

Prof. T. Wu
Department of Applied Physics, the Hong Kong Polytechnic University, Kowloon, Hong Kong 999077, China.

1. Materials

1-octandecene (ODE, 90%, J&k), oleic acid (OA, 90%, Alfa), oleylamine (OAm, 90%, Alfa), formamidine acetate (FAAc, 99.9%, Alfa), lead iodide (PbI_2, 99.9%, Sigma), n-hexane (97.5%, J&K), n-octane (anhydrous, ≥ 98%, Alfa), MeOAc (anhydrous, 99.5%, Sigma), methylamine hexafluorophosphate ($MAPF_6$, ≥ 98%, Macklin), isopropanol (IPA, 99%, J&k), methylamine iodide (MAI, 99.0%, Greatcell), titanium tetrachloride ($TiCl_4$, >98%, Sinopharm Chemical Reagent Co., Ltd.), tris(pentafluorophenyl)borane (LAD, 95%, Acros Organics), and poly(triarylamine) (PTAA, 99.9%) were purchased from Xi'an Polymer Light Technology Corp. (China). All the materials were used directly without further purification. Glass/FTO were purchased from Advanced Election Technology Co., Ltd (China).

2. Characterizations

The TEM images were recorded by a Tecnai G2 F20 S-Twin system operated at 200 kV. UV-vis absorption spectra were collected by using a PerkinElmer model Lambda 750 spectrophotometer with a step of 2 nm. PLQY of PQDs solution were obtained through the absolute PL quantum yield spectrometer. PL spectra were obtained by using a Fluorescence Spectrometer (NIR-VIS, FL3). TRPL spectra were measured using a Hamamatsu streak camera. *In-situ* PL spectra were measured by FX2000-EX (Ideaoptics) with excitation wavelength at 400 nm. SEM images were obtained from a HETACHI SU8230 field emission scanning electron microscope. XPS and UPS measurements were performed on a Kratos AXIS Ultra DLD ultrahigh-vacuum photoemission spectroscopy system equipped with an Al-Kα (1,486.6 eV). FTIR spectra were analyzed on a Bruker HYPERION FTIR spectrometer and cumulated 32 scans at a resolution of 3 cm^{-1}. AFM and KPFM images were obtained using a Bruker Dimension Icon SPM system. The 2D PL mapping images were obtained

using a confocal Raman imaging system (Alpha300R) with a laser source. The fs-TA was measured with an ultrafast surface Xplorer system. Crystal structure, orientation and stacking structure of PQD film were obtained by XRD (Rigaku D/Max-Ra X-ray diffractometer with a monochrome at Cu Kα radiation (λ~1.54 Å)) and GIWAXS (Shanghai Synchrotron Radiation Facility Laboratory on Beamline BL14B1 using X-rays with a wavelength of λ ≈ 1.24 Å). EQE measurement of the solar cells was characterized on a Solar Cell Scan 100 system (Zolix Instruments). Drive-level capacitance profiling, transient photovoltage, electrochemical impedance spectroscopy, and Mott-Schottky plots measurements were performed using a Zahner IM6 electrochemical workstation.

The active area of 0.0725 cm^2 or 1.02 cm^2 was defined by a shadow mask, and an aperture mask of 0.04 cm^2 or 1 cm^2 was used during the test. *J–V* curves of the devices were measured by a Keithley 2400 Digital Source Meter under N_2 glovebox and simulated AM 1.5 G spectrum at 100 mW cm^{-2} (certified by a monocrystalline silicon reference cell (91150V, Newport Oriel)) with a solar simulator (Class AAA, 94023A-U, Newport). *J–V* scans were measured by the forward direction (−1.30 to 1.30 V) and reverse direction (1.30 to −1.30 V) with a speed of 0.016 V per point and a scan rate of 0.1 V s^{-1}.

3. TRPL measurements

The PL decay curves of PQDs in solution phase was fitted using a bi-exponential equation,

$$I_{(t)} = A_1 * \exp\left(-\frac{t}{\tau_1}\right) + A_2 * \exp\left(-\frac{t}{\tau_2}\right) + A_0,$$

where A_1, A_2 and A_0 are constant, t is *PL* decay time, τ_1, τ_2 are fitted lifetimes. The τ_{ave} was calculated using the following equation,

$$\tau_{ave} = \frac{A_1\tau_1^2 + A_2\tau_2^2}{A_1\tau_1 + A_2\tau_2}.$$

The PL decay curves of PQD films was fitted using a tri-exponential equation,

$$I_{(t)} = A_1 * \exp\left(-\frac{t}{\tau_1}\right) + A_2 * \exp\left(-\frac{t}{\tau_2}\right) + A_3 * \exp\left(-\frac{t}{\tau_3}\right) + A_0,$$

where A_1, A_2, A_3 and A_0 are constant, t is PL decay time, τ_1, τ_2, τ_3 are fitted lifetimes. The τ_{ave} was calculated using the following equation,

$$\tau_{ave} = \frac{A_1\tau_1^2 + A_2\tau_2^2 + A_3\tau_3^2}{A_1\tau_1 + A_2\tau_2 + A_3\tau_3}.$$

The carrier diffusion distance L_D was calculated using the equation:

$$\frac{L_D}{L} = \frac{2}{\pi}\sqrt{\frac{1}{\tau_Q/\tau_0} - 1},$$

where L is the thickness of PQD film, τ_Q is the quenching lifetime, τ_0 is the intrinsic life.

4. Film conductivity measurement

The film conductivity measurement with a device structure of FTO/PQD/Ag was recorded by Keithley 2400 and measured under dark conditions. The corresponding conductivity of $FAPbI_3$ PQD films can be calculated by the following equation:

$$\sigma = \frac{JL}{V}$$

Where J, V, σ and L are current density, voltage, conductivity and active layer film thickness (400 nm), respectively.

5. Film SCLC measurements

The electron-only device structure is glass/FTO/TiO_2/PQDs/PCBM/Ag. The electronic trap density (n_t) of $FAPbI_3$ PQD film was calculated by the following equation:

$$n_t = \frac{2\varepsilon_0\varepsilon_r V_{TFL}}{eL^2},$$

Where ε_0, ε_r, V_{TFL}, e and L are vacuum permittivity, the dielectric constant, trap-filled limit voltage, elementary charge and film thickness, respectively.

The electron mobility is calculated using Mott-Gurney formula:

$$\mu_e = \frac{8JL^3}{9\varepsilon_0\varepsilon_r V^2},$$

Where J is the current density from the SCLC region and V is the applied voltage.

6. TPV measurements

The V_{OC} decay was fitted using a bi-exponential equation,

$$V_{OC} = A_1 * \exp\left(-\frac{t}{\tau_1}\right) + A_2 * \exp\left(-\frac{t}{\tau_2}\right) + A_0,$$

where A_1, A_2, and A_0 are constant, t is V_{OC} decay time, τ_1, τ_2 are fitted lifetimes. The τ_{ave} was calculated using the following equation,

$$\tau_{ave} = \frac{A_1\tau_1^2 + A_2\tau_2^2}{A_1\tau_1 + A_2\tau_2}.$$

7. Temperature EIS measurements

The obtained Nyquist plot of the temperature EIS measurements shows two different charge transport regions. The semi-circle close to the origin is associated with a higher frequency spectrum, which is mainly attributed to the impedance generated by electron transport. The linear region is associated with the low spectrum and is attributed to the impedance caused by ion migration. The Nyquist diagram fitted into the circuit model, including high-frequency electronic components and low-frequency ionic components, and obtained the Warburg time constant (T_w) using ZView version 3.4c. Then perform linear fitting on $\ln[(T_w \times T)^{-1}]$ and 1000/T. The activation energy (E_a) of ion migration can be calculated using the equation,

$$\frac{1}{T_w} = \frac{kT}{h}\frac{a^2\alpha}{L_D^2}\exp(-\frac{E_a}{kT}),$$

where k is the Boltzmann constant and T is the absolute temperature. L_D is the lattice parameter of perovskite, α is the coordination factor, and h is the Planck's constant.

8. First-principles calculations

Density functional theory (DFT) calculations were performed to theoretically characterize the structural and binding properties of the OA and PF_6 on pristine and defective $FAPbI_3$ surfaces.[1] The PBE exchange-correlation energy functional [2] was used as it is implemented in the VASP software,[3] and dispersion long-range interactions were described with the DFT+D3 correction method due to Grimme et al.[4] The "projector augmented wave" method[5] was employed to represent the ionic cores by considering the following electrons as valence: Pb 6s, 5d and 6p; I 5s and 5p; P 3s and 3p; F 2s and 2p; C 2s and 2s; N 2s and 2s; O 2s and 2p; H 1s. Wave functions were represented in a plane-wave basis truncated at 650 eV. For integrations within the first Brillouin zone, we employed Monkhorst-Pack k-point grids with a density equivalent to that of a 12x12x12 mesh for the $FAPbI_3$ unit cell. Molecular binding energies were estimated by subtracting the energy of the isolated molecular and $FAPbI_3$ surface systems to that of the combined molecule@ $FAPbI_3$ surface system.

Periodic boundary conditions were applied along the three lattice vectors defining the simulation supercell. Geometry relaxations were performed with a conjugate-gradient algorithm that optimized the ionic positions and shape of the simulation cell. The relaxations were halted when the forces in the atoms were all below 0.005 eV·Å-1. By using these technical parameters, total energies were converged to within 0.5 meV per atom. The $FAPbI_3$ slab calculations were performed using large supercells (256 atoms) with a 2.5 nm thick vacuum region. The molecular OA and PF_6 adsorption simulations were performed considering the (001) $FAPbI_3$ surface.

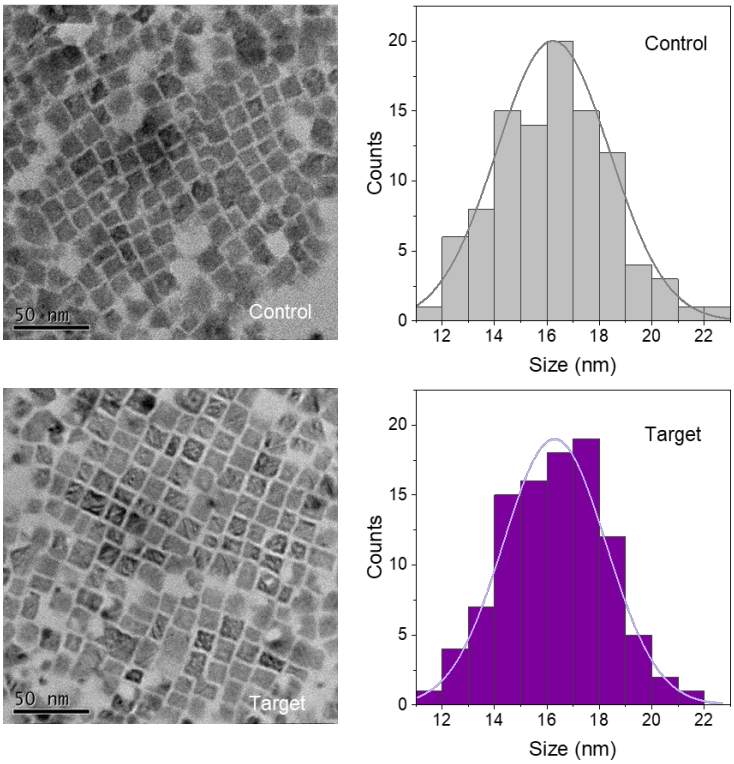

Figure S1. TEM spectra and size distribution of different PQDs.

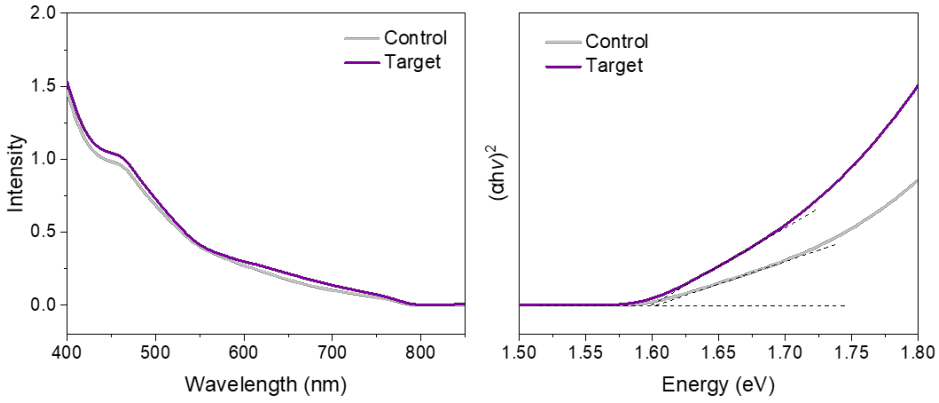

Figure S2. Absorption spectra (left) and tauc (right) plots of different PQDs.

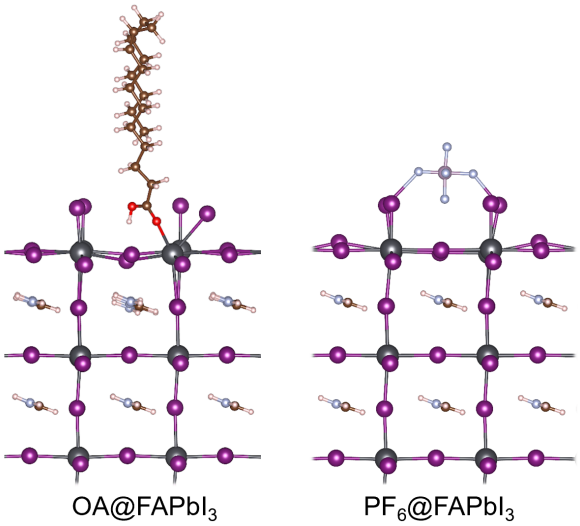

Figure S3: Equilibrium geometries determined with first-principles DFT methods. OA and PF_6 molecule adsorbed on $FabI_3$ surfaces. White, red, brown, dark purple, blue, light purple, and grey spheres represent H, O, C, I, N, P and Pb atoms, respectively.

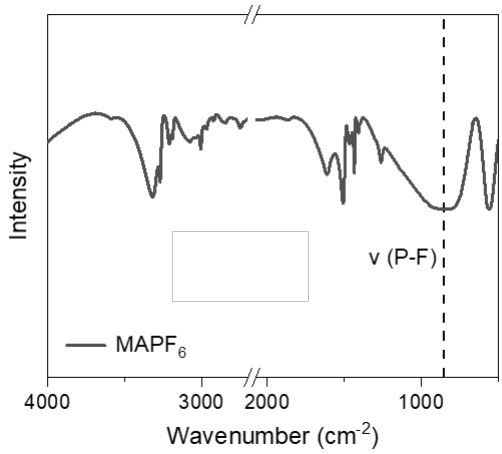

Figure S4. The FTIR spectra of pure $MAPF_6$.

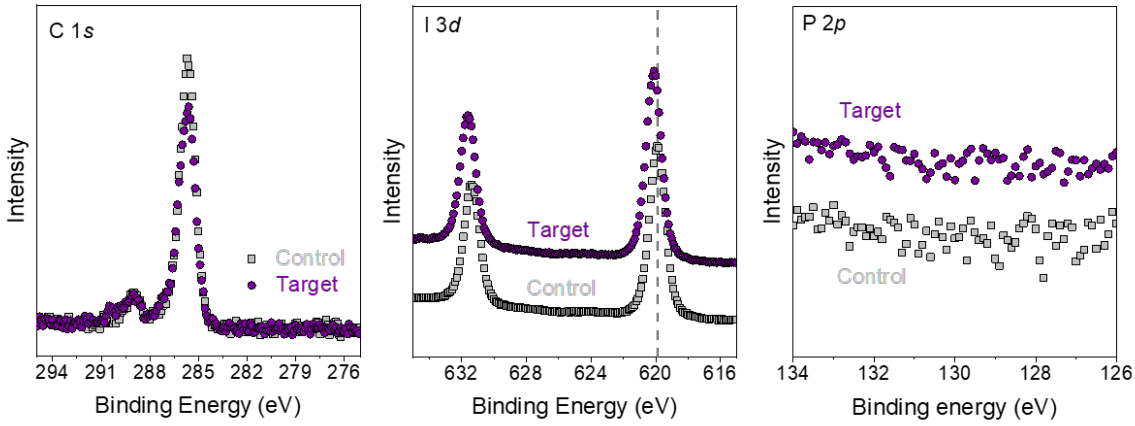

Figure S5. The XPS spectra of C 1*s* and P 2*p* of different PQDs.

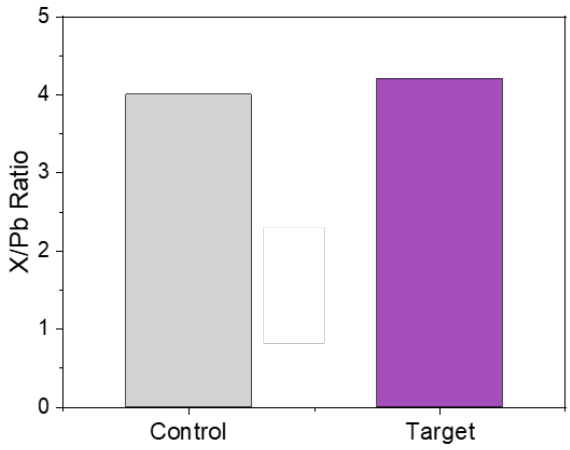

Figure S6. Relative X/Pb elemental ratio of different PQDs.

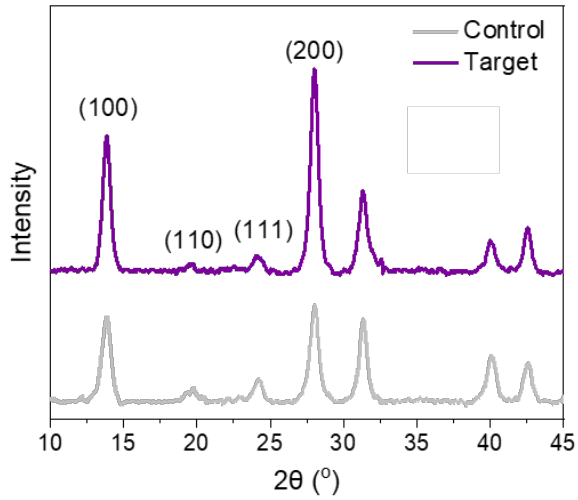

Figure S7. XRD pattern of the control and target PQD films.

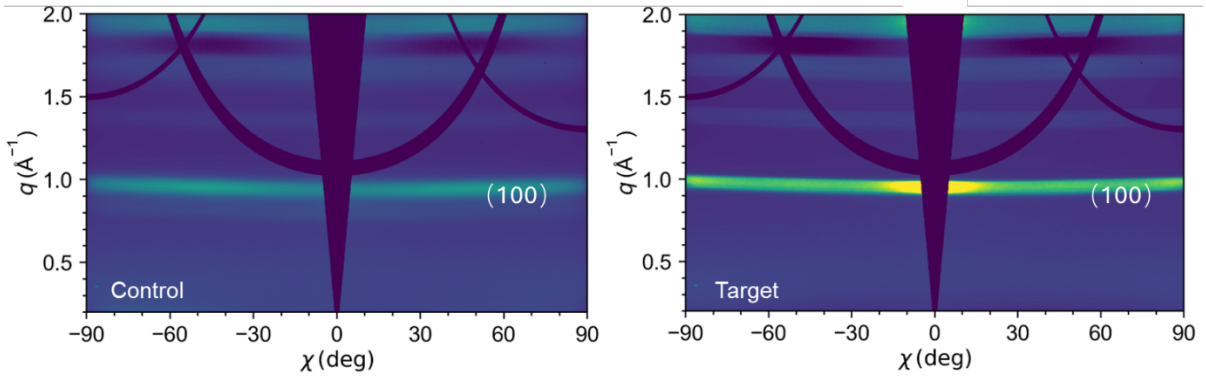

Figure S8. Azimuthal integration of the (100) peak of the control and target film.

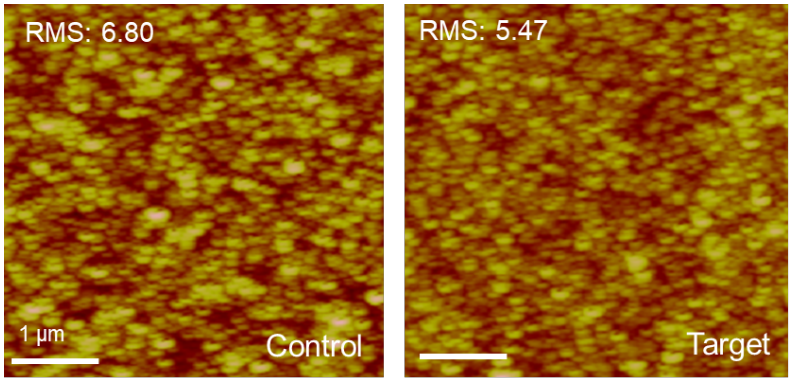

Figure S9. AFM height images of the control and target films.

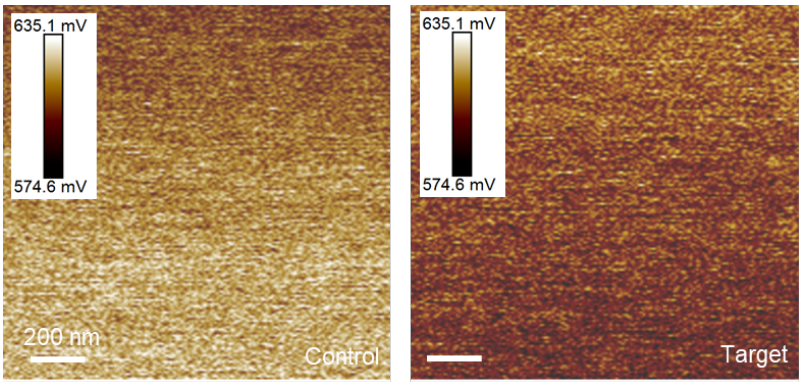

Figure S10. KPFM images of the control and target films.

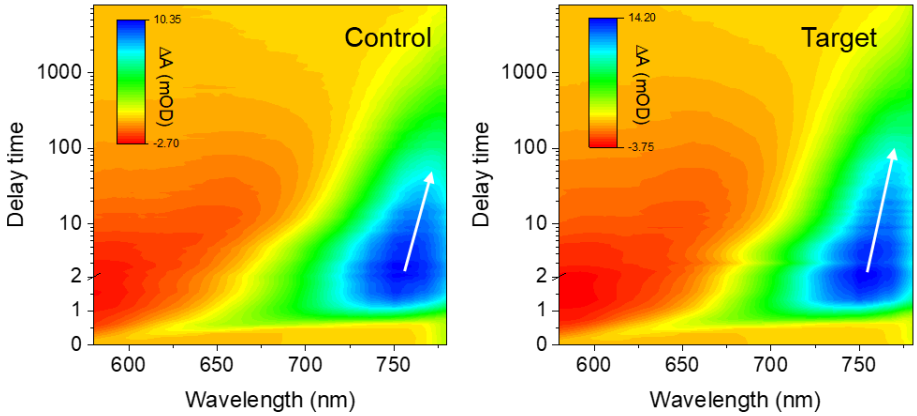

Figure S11. TA spectra and the corresponding GSB decay spectra of different PQD films.

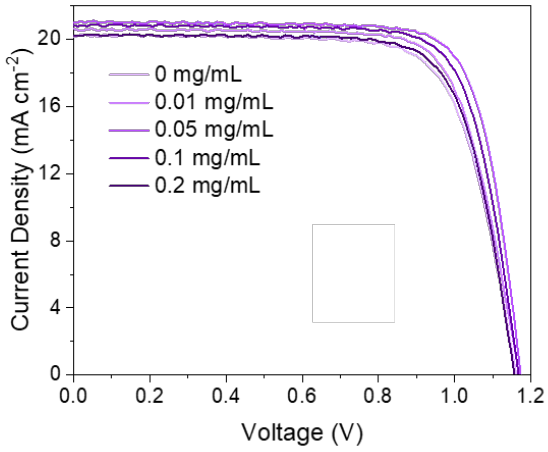

Figure S12. *J-V* curves of the target PQD solar cells treated by different concentration of $MAPF_6$.

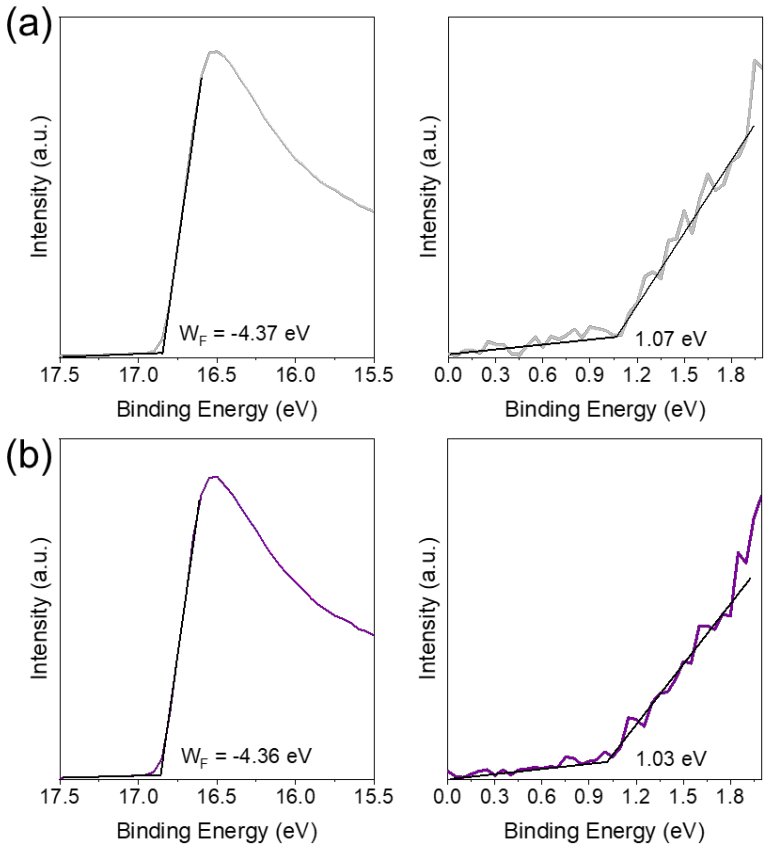

Figure S13. UPS plots of (a) control and (b) target PQDs. Left and right figures show the secondary electron cut-off region and valence band region, respectively.

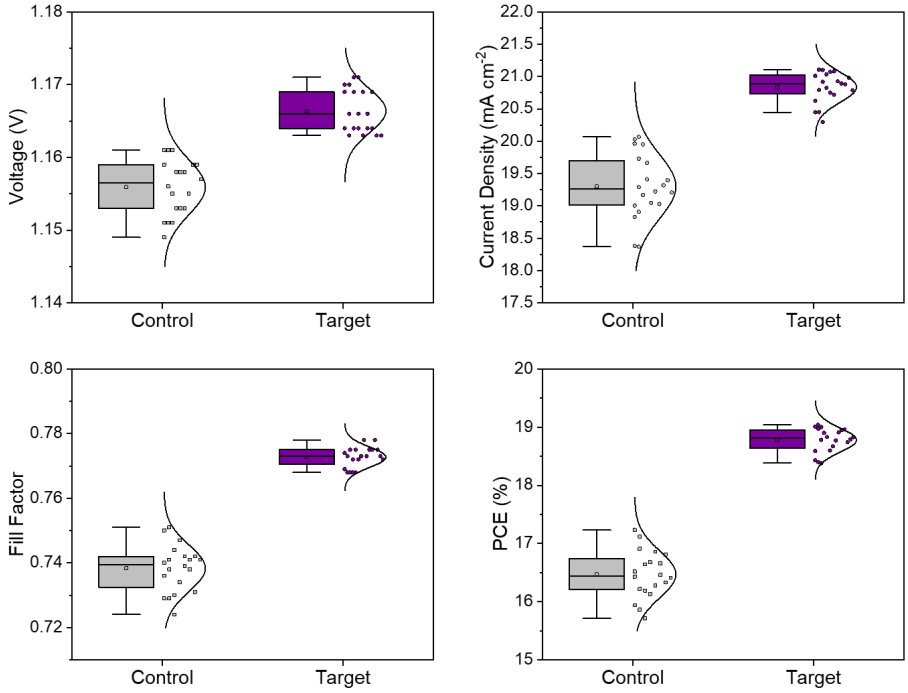

Figure S14. Statistics of the PCE, V_{OC}, FF, and J_{SC} of the devices obtained from the *J-V* curves of the 20 devices.

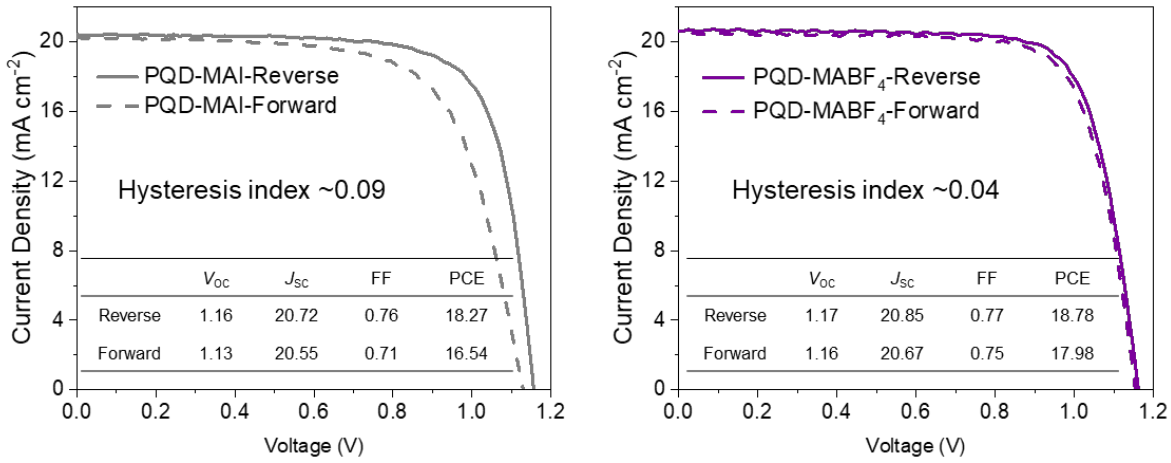

Figure S15. *J-V* curves of MAI and $MABF_4$ treated PQD devices.

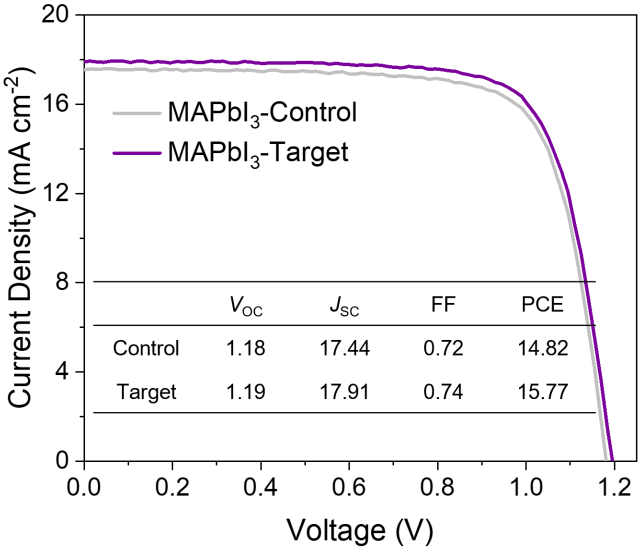

Figure S16. *J-V* curves of $MAPbI_3$ PQD based control and target devices.

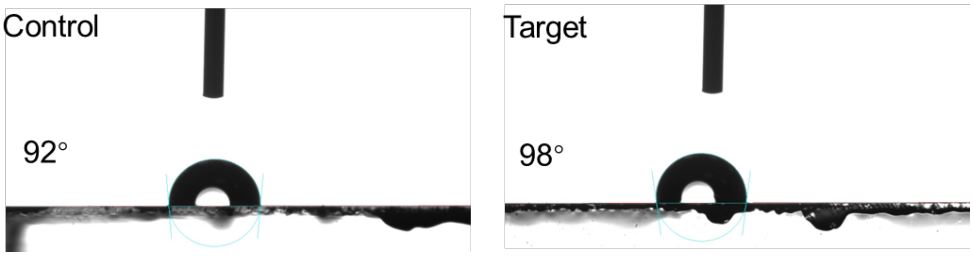

Figure S17. Water contact angle of different PQD films.

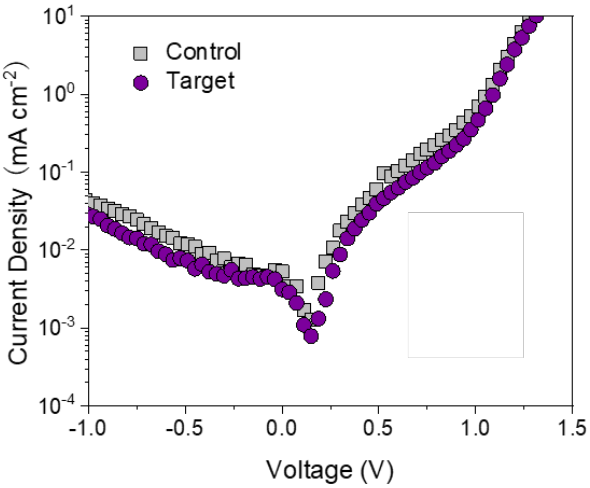

Figure S18. Dark current of different PQD devices.

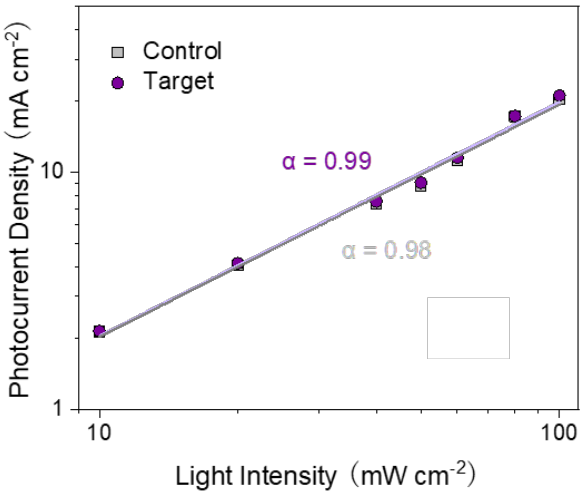

Figure S19. Light intensity-dependent photocurrent density plots of different PQD devices.

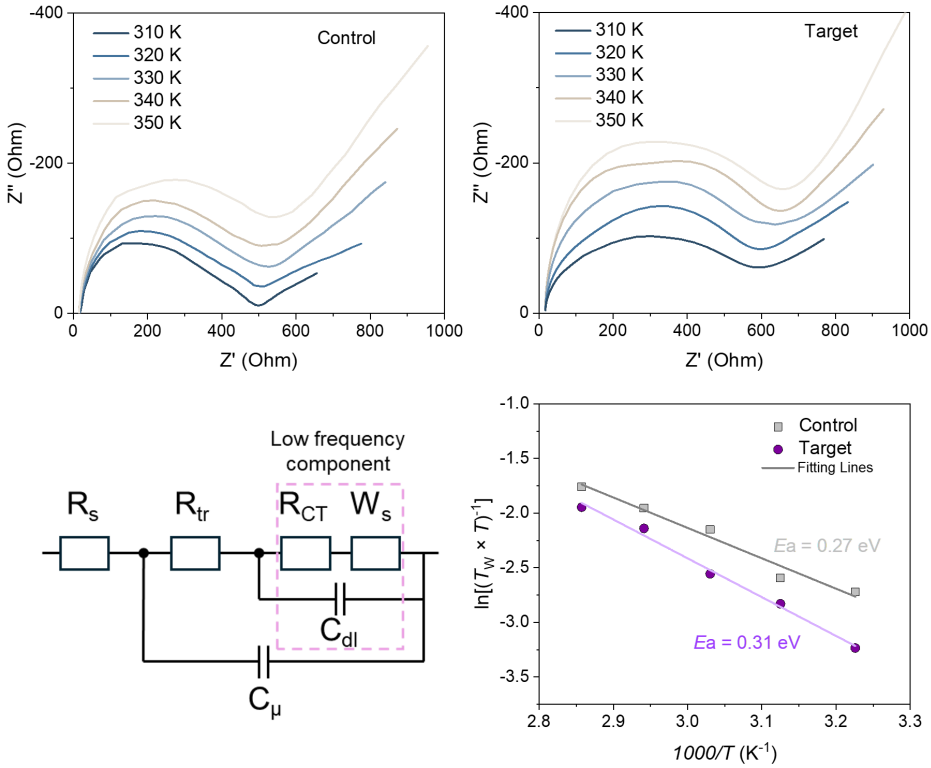

Figure S20. Temperature dependent impedance plot of control and target devices under 1 sun and 0 V applied bias. Corresponding equivalent circuit diagram of devices showing combined charge and ion transport impedance and the Arrhenius-like plot for control and target devices.

Table S1. The detailed parameters of TRPL spectra of $FAPbI_3$ PQDs in solution phase.

Sample	A_1	τ_1 (ns)	A_2	τ_2 (ns)	τ_{ave} (ns)
Control	0.53	15.67	0.47	112.00	98.87
Target	0.45	18.13	0.55	121.57	110.32

Table S2. The detailed parameters of TRPL spectra of $FAPbI_3$ PQDs on FTO/TiO_2 substrates.

Sample	A_1	τ_1 (ns)	A_2	τ_2 (ns)	A_3	τ_3 (ns)	τ_{ave} (ns)
Control	0.69	1.09	0.27	4.18	0.04	15.08	5.89
Target	0.71	0.97	0.25	3.74	0.04	13.82	5.42

Table S3. The detailed parameters of TRPL spectra of $FAPbI_3$ PQDs on quartz substrates.

Sample	A_1	τ_1 (ns)	A_2	τ_2 (ns)	A_3	τ_3 (ns)	τ_{ave} (ns)
Control	0.54	1.82	0.38	8.12	0.08	32.89	16.92
Target	0.52	1.99	0.39	8.87	0.09	35.25	18.86

Table S4. The parameters in TA spectra of $FAPbI_3$ PQD films.

Sample	A_1 (%)	τ_1 (ps)	A_2 (%)	τ_2 (ps)	A_3 (%)	τ_3 (ps)	τ_{ave} (ps)
Control	27.13	13.15	47.35	101.87	25.52	827.49	683.35
Target	24.15	8.68	45.61	114.34	30.24	961.06	827.23

Table S5. The detailed *J–V* parameters of different concentration of $MAPF_6$ treated PQD solar cells.

Sample	V_{OC} (V)	J_{SC} (mA cm^{-2})	FF	PCE (%)
Control (0 mg/mL)	1.159	20.03	0.742	17.23
$MAPF_6$ 0.01 mg/mL	1.165	20.73	0.764	18.45
$MAPF_6$ 0.05 mg/mL	1.169	21.09	0.771	19.01
$MAPF_6$ 0.1 mg/mL	1.163	20.93	0.770	18.74
$MAPF_6$ 0.2 mg/mL	1.155	20.14	0.758	17.63

Table S6. The detailed *J–V* parameters of device performance for control and target devices.

Sample		V_{OC} (V)	J_{SC} (mA cm^{-2})	FF	PCE (%)
Control	Champion	1.159	20.03	0.742	17.23
	Average[a]	1.156±0.004	19.29±0.49	0.738±0.007	16.47±0.40
Target	Champion	1.169	21.09	0.771	19.01
	Average	1.166±0.003	20.83±0.23	0.773±0.004	18.78±0.21

[a] The average data based on 20 devices.

Table S7. The fitted parameters of the TPV curves of control and target PQD solar cells.

Sample	A_1	τ_1 (μs)	A_2	τ_2 (μs)	τ_{ave} (μs)
Control	0.48	0.13	0.35	2.27	2.11
Target	0.34	0.15	0.43	2.86	2.75

Table S8. The fitted parameters of the EIS of control and target PQD solar cells.

Sample	R_s (Ω)	R_{rec} (Ω)
Control	26.6	1140.9
Target	21.7	1530.3

[1] C. Cazorla, J. Boronat, *Rev. Mod. Phys.* **2017**, *89*, 035003.
[2] J. P. Perdew, A. Ruzsinszky, G. I. Csonka, O. A. Vydrov, G. E. Scuseria, L. A. Constantin, X. Zhou, K. Burke, *Phys. Rev. Lett.* **2008**, *100*, 136406.
[3] G. Kresse, J. Furthmüller, *Phys. Rev. B* **1996**, *54*, 11169.
[4] S. Grimme, J. Antony, S. Ehrlich, H. Krieg, *J. Chem. Phys.* **2010**, *132*, 154104.
[5] P. E. Blöchl, *Phys. Rev. B* **1994**, *50*, 17953.